Non-Newtonian flow effects on the coalescence and mixing of initially stationary droplets of shear-thinning fluids

Kai Sun,[1,2] Tianyou Wang,[1] Peng Zhang,[2,*] and Chung K. Law[3,4]
[1]*State Key Laboratory of Engines, Tianjin University, Tianjin, China*
[2]*Department of Mechanical Engineering, The Hong Kong Polytechnic University, Hong Kong*
[3]*Center for Combustion Energy, Tsinghua University, Beijing, China*
[4]*Department of Mechanical and Aerospace Engineering, Princeton University, Princeton, New Jersey, USA*
(Received 13 August 2014; published 12 February 2015)

The coalescence of two initially stationary droplets of shear-thinning fluids in a gaseous environment is investigated numerically using the lattice Boltzmann method, with particular interest in non-Newtonian flow effects on the internal mixing subsequent to coalescence. Coalescence of equal-sized droplets, with one being Newtonian while the other is non-Newtonian, leads to the non-Newtonian droplet wrapping around the Newtonian one and hence minimal fine-scale mixing. For unequal-sized droplets, mixing is greatly promoted if both droplets are shear-thinning. When only one of the droplets is shear-thinning, the non-Newtonian effect from the smaller droplet is found to be significantly more effective than that from the larger droplet in facilitating internal jetlike mixing. Parametric study with the Carreau-Yasuda model indicates that the phenomena are universal to a wide range of shear-thinning fluids, given that the extent of shear thinning reaches a certain level, and the internal jet tends to be thicker and develops more rapidly with increasing extent of the shear-thinning effect.

DOI: 10.1103/PhysRevE.91.023009 PACS number(s): 47.11.−j, 47.50.−d, 47.55.df

I. INTRODUCTION

Coalescence of colliding droplets in gaseous environment is of fundamental interest to many natural and industrial processes such as rain drop and cloud formation, atmospheric aerosol circulation, and spray painting and combustion. Through experimental investigation [1–7], numerical simulation [8–17], and theoretical analysis [18], much understanding has been acquired on the collision outcome, including coalescence, bouncing, and separation.

Recent research in microfluidics and propulsion systems involving the liquid-phase reaction has led to the interesting question on the fate of the internal fluids following droplet coalescence. A prominent example is the ignition of gelled hypergolic propellants in rocket engines. Specifically, the gelled fuel and the oxidizer are sprayed separately into the combustion chamber, leading to the subsequent collision between the embedded droplets. Because of the low vapor pressure of the gelled propellant, ignition only can be triggered, in the liquid phase, after the fuel and oxidizer droplets come into permanent coalescence and followed by sufficient and rapid mixing [19]. Subsequently, unraveling and promoting the internal mixing mechanism is central to the viability of the utilization of gelled bipropellants.

Studies on droplet mixing have mainly focused on unequal-sized droplets as internal mixing of equal-sized droplets of the same fluid is minimal due to symmetry. Specifically, Anilkumar *et al.* [20] and Law *et al.* [19,21] experimentally studied the permanent coalescence at low Weber numbers ($\mathrm{We} = \rho_d U^2 D_s/\sigma$, where ρ_d is the density of the droplet, U the relative velocity between the droplets, D_s the diameter of the smaller droplet, and σ the surface tension) and observed considerable internal mixing in the forms of jet or vortex ring for low-viscosity liquids. Ashgriz and Poo [3] experimentally investigated the mass exchange during collision at high Weber numbers and showed that the mass in the smaller droplet generated from the "reflexive separation" of the temporarily coalesced droplet actually originates from the initially larger one. Nobari and Tryggvason [22] simulated the coalescence of two initially stationary droplets and observed jetlike mixing at low Ohnesorge numbers ($\mathrm{Oh} = \mu_d/\sqrt{\rho_d \sigma D_s}$, where μ_d is the dynamic viscosity of the droplet), while Liu *et al.* [23] showed for the same momentumless situation that disparity in the droplet sizes is critical in affecting the mixing efficiency. Furthermore, Nikolopoulos *et al.* [11,12], Sun *et al.* [14], and Chen *et al.* [17] also computationally showed that the mixing characteristics are sensitive to the size ratio, the Weber number, and the Ohnesorge number. Recently, Blanchette [24] numerically observed significant mixing between two equal-sized droplets with different surface tensions as a result of the Marangoni effect, although it is generally recognized that mixing between equal-sized droplets is greatly restricted by the geometric symmetry.

Compared to the large number of investigations on the droplet collision of Newtonian fluids, relatively few studies have been conducted for non-Newtonian fluids, which are of relevance to, for example, polymers. Specifically, Motzigemba *et al.* [25] experimentally observed substantially larger deformation upon the collision of two droplets of shear-thinning fluids as compared to that for Newtonian fluid. Focke and Bothe [26,27] numerically found that the collision dynamics of non-Newtonian droplets at high Weber number in the range of 357–766 can be reproduced by that of Newtonian droplets with an effective constant viscosity, which, however, is neither the mean nor the minimum value. Recently, the collision between two droplets with distinctly different viscosities was investigated by Focke *et al.* both experimentally and numerically [28]. A pressure jump across the liquid-liquid interface within the coalesced droplet was observed and attributed to the viscosity

*To whom correspondence should be addressed: pengzhang.zhang@polyu.edu.hk

jump across the same interface. It is nevertheless noted that, in spite of these worthy advances, a detailed investigation on the internal mixing within coalesced non-Newtonian droplets has not been attempted. It is of particular interest to explore whether non-Newtonian effects can facilitate internal mixing, especially for equal-sized droplets, and whether it is able to substantially relieve the suppression of viscosity on the mixing for unequal-sized droplets.

In the present investigation, we aim to numerically study the non-Newtonian effects on the coalescence of two initially stationary droplets, with emphasis on the internal mixing processes. Only shear-thinning fluids are considered because of their relevance to gelled hypergolic propellants for propulsion and polymers in industrial applications. The coalescence of droplets with finite initial velocity is not considered because the additional physics of gas-film drainage must be corrected taken into account in the difficult problem. In addition, numerically resolving the extremely thin air gap separating the droplets at high Weber numbers is computationally demanding because the gap distance could be as small as $O(10^2)$ Å before coalescence occurs [6,18], which is four orders of magnitude smaller than the droplet diameters considered in the present study. Furthermore, the present problem is an approximation of low Weber number collision, which is frequently seen in reality.

The rest of the paper is organized as follows: In Sec. II, the numerical method is briefly described, in Sec. III, simulation results are presented and discussed, and conclusions are given in Sec. IV.

II. NUMERICAL METHODS

When two droplets are placed adjacent to each other, the interfaces will merge once they come into contact at a point. Driven by surface tension, substantial internal motion will be generated within the entire coalesced mass as it attempts to achieve sphericity, leading to mixing as well as viscous dissipation. Since the droplets are momentumless, the problem is intrinsically axisymmetric with the axis of symmetry passing through both centers of the spherical droplets.

In the present study, the lattice Boltzmann method (LBM) is used to simulate the droplet dynamics, while the mixing process following droplet coalescence is visualized by tracking massless particles inside the droplets. The particle trajectories are computed using the fourth-order Runge-Kutta method. The details of the numerical methods have been fully described in the authors' previous paper [14] and as such they will only be briefly summarized here. In the LBM simulation, one distribution function is used to track the composition of the two-phase mixture, while another is employed to compute the dynamic pressure that enforces incompressibility [29]. It should be noted that although LBM is generally known for its spurious current near the interface, the present multiphase model is able to suppress the spurious current to a relatively low level even at high density ratios, which is achieved through the implementation of the potential form of the surface tension and the isotropic finite difference [30]. To further improve the numerical stability for the simulation of low-viscosity flows, the widely used extension of the LBM multiphase model to the multiple-relaxation-time (MRT) scheme was also adopted in the authors' previous paper [14]. Based on the authors' observations, the LBM model with the MRT extension did not show significant numerical instability when the kinematic viscosity $\nu = \tau c_s^2$ is as small as $O(10^{-4})$, which enables us to study droplet coalescence at very small Ohnesorge numbers.

Differing from previous LBM simulations for Newtonian fluids with constant viscosities, the variation of viscosity with the local shear rate has to be taken into account for the non-Newtonian effects. This was achieved by replacing the constant relaxation time in the classical Bhatnagar-Gross-Krook (BGK) model by one that is shear-rate dependent [31–34]. For the present simulation based on the MRT model, the relaxation parameter s_ν in the collision matrix $\Lambda = \mathrm{diag}(s_\rho, s_e, s_\varepsilon, s_j, s_q, s_j, s_q, s_\nu, s_\nu)$ is modified to depend on the local shear rate. In addition, the shear-rate-dependent viscosity should be also used in the related equations in Ref. [14], which explicitly contain viscosity. In the present computational procedure, after the liquid-gas interface is captured by the LBM multiphase model, the local fluid can be distinguished as either Newtonian or non-Newtonian by tracking particles. If the local fluid is non-Newtonian, the calculation of viscosity-related terms would use the shear rate-dependent viscosity $\mu = \mu(\dot\gamma)$ instead of constant viscosity.

As one of the most widely applied constitutive equations for shear-thinning fluids, the Carreau-Yasuda model, given by

$$\mu(\dot\gamma) = \mu_\infty + (\mu_0 - \mu_\infty)[1 + (\lambda_{CY}\dot\gamma)^a]^{(n-1)/a}, \qquad (1)$$

is used in the present study, where μ_0 and μ_∞ are the dynamic viscosity at zero and infinite shear rates, respectively, λ_{CY} is a time constant, n a power-law index, and a a parameter affecting the transition between the zero-shear rate and power-law regions [35]. In the LBM simulation, since all variables are defined in lattice unit (LU) rather than physical unit (PU), λ_{CY} in Eq. (1) is transformed to $\lambda = \lambda_{CY} T_{OSC(LU)}/T_{OSC(PU)}$, where $T_{OSC} = (\pi/4)\sqrt{\rho_l R_s^3/\sigma}$ is the characteristic oscillation time of the smaller droplet. It is noted that the present simulation is not restricted to any specific non-Newtonian fluid; Eq. (1) is adopted because it is a prevalent model for shear-thinning fluids. Other constitutive equations such as the Cross model [35] can be implemented in the same way, and our simulation results indicate that they do not cause any qualitative difference. In the rest of the paper, the parameters in Eq. (1) are first fixed to be $n = 0.5$, $a = 0.557$, and $\lambda_{CY}/T_{OSC} = 61.9$, corresponding to a kind of carboxymethyl cellulose solution [35], and the dependence of the results on the extent of shear-thinning effect will be also discussed. Constant surface tension is assumed for the two droplets consisting of either Newtonian or non-Newtonian fluid. The dilution of the shear-thinning effect due to mass diffusion between the droplets is neglected, as the Peclet number, defined by $\mathrm{Pe} = UL/D$ (where U is the characteristic velocity, L the characteristic length, and D the mass diffusivity between different liquids), is generally on the order of 10^5 in the present situation if U and L are chosen to be D_s/T_{OSC} and D_s, respectively.

From dimensional analysis, four nondimensional parameters are needed to describe the correct flow similarity, namely the large-to-small droplet size ratio $\Delta = D_l/D_s$, the droplet-to-ambient fluid density ratio ρ_d/ρ_a, the droplet-to-ambient

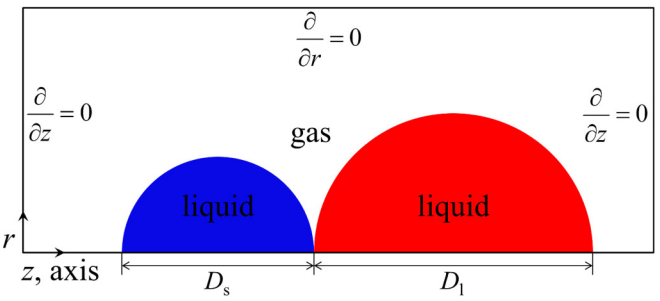

FIG. 1. (Color online) Specifications of computational domain and boundary conditions.

fluid viscosity ratio μ_d/μ_a, and the Ohnesorge number based on the diameter of the smaller droplet. For the shear-thinning fluid, Oh and Oh_∞ will designate the Ohnesorge number at zero and infinite shear rates, respectively. Since the present study focuses on droplet coalescence in gaseous environment of nearly atmospheric pressure, both ρ_d/ρ_a and μ_d/μ_a are too large to have significant influence on the results, as substantiated in previous studies [4–6]. Therefore, ρ_d/ρ_a and μ_d/μ_a are kept constant at 833 and 55.6, respectively, in the simulation (corresponding to water droplets in air), and Δ and Oh will be the controlling parameters in the following. Finally, time t is nondimensionalized as $T = t/T_{\mathrm{OSC}}$.

As shown in Fig. 1, the present simulation is carried out in an axisymmetric domain, where the axisymmetric boundary condition (BC) is imposed on the axis, with Neumann BC of zero gradients for all the variables applied on the other boundaries. In the computation, the numerical diffuse interface thickness of droplet is set to be five lattice spacing. Initially, two droplets are placed close to each other so one-fifth (i.e., one lattice spacing) of their diffuse interfaces is overlapped. Since the overlapped interfaces are not in equilibrium, they will automatically merge and expands radially so as to minimize the free energy. According to our test, the coalescence and drainage process is not significantly affected by the numerical thickness of the interface for R_s (the number of lattice spacing per the smaller droplet radius) greater than 50. Furthermore, grid independence study has been also conducted in comparison with the experiment by Law *et al.* [19,21], showing that 70 lattice spacing per the smaller droplet radius is sufficient to resolve both the droplet dynamics and the mixing process. Therefore, $R_s = 70$ (lattice spacing) is used to produce the results discussed in the following.

III. RESULTS AND DISCUSSION

A. Experimental verification

To the knowledge of the authors, no experimental data of coalescence and internal mixing of non-Newtonian droplets are available in literature. Therefore, the direct comparison of the present simulation with experiment cannot be given in this paper. To validate the present numerical method, coalescence between two Newtonian droplets is simulated and compared with the experiments of Anilkumar *et al.* [20] and of Law *et al.* [19,21]. Figure 2(a) shows two levitated droplets of the mixture of silicon oil and bromobenzene merging in water, with $\Delta = 2.08$. Considering that the experimental Ohnesorge number is not clearly specified in Ref. [20] and that Oh may vary in the range of $0.010 \sim 0.015$ depending on the unspecified interfacial tension between the mixture and water, we used $\mathrm{Oh} = 0.012$ and found that our simulation agreed well with the experiment in both the droplet shape evolution and internal jet formation, irrespective of some minor differences in the time sequence. Figure 2(b) shows two highly viscous silicone oil droplets merging in water at $\Delta = 1.75$ and $\mathrm{Oh} = 0.203$. The simulation also agrees well with the experiment, as the smaller droplet lodges onto the larger one, forming a dome at such a high Ohnesorge number. Figure 2(c) shows two water droplets merging in air at $\Delta = 1.87$ and $\mathrm{Oh} = 0.006$, for which the simulation also captures qualitatively the droplet deformation and internal mixing, although it generally evolves slightly faster than the experiment. It is noted that the droplets collide at a nonzero albeit small Weber number ($\mathrm{We} = 0.47$) in the experiment shown in Fig. 2(c), implying the actual coalescence instant in the experiment is slightly behind that in the simulation because the drainage of the gas film separating the droplets requires additional time. Overall, the numerical method has proven its capability to handle the present problem, justifying further simulation as follows.

B. Coalescence between equal-sized droplets

First, the coalescence of two equal-sized droplets is considered. As discussed in the Introduction, the coalescence between identical Newtonian droplets always results in a symmetric contact plane. This feature also holds for identical non-Newtonian droplets because the local viscosity is also symmetrical. To break the symmetry, the coalescence between a non-Newtonian droplet and a Newtonian droplet is expected to result in active mixing patterns.

Figure 3 shows two cases of coalescence between a Newtonian droplet (red, upper) and a non-Newtonian droplet (blue, lower), at two Ohnesorge numbers. The mixing process is illustrated in the left half of the images while the right half shows the variation of local dynamic viscosity, normalized by the initial value μ_0 at zero shear rate. Initially, the dynamic viscosity of the non-Newtonian droplet is identical to the Newtonian one. However, it will vary according to Eq. (1) as the droplets merge and deform. Figure 3(a) shows the case of $\mathrm{Oh} = 0.01$ and $\mathrm{Oh}_\infty = 0.0015$, where asymmetric mixing is observed with the non-Newtonian droplet tending to wrap around the Newtonian droplet. This phenomenon can be explained as follows. During the first stage of droplet coalescence, i.e., from the instant of interface rupture to that of the formation of a radial bulge ($T = 0.00 \sim 1.10$), the contact surface between the droplets expands radially, driven by surface tension, and a counterflow of large shear rate towards the symmetric plane is induced in each droplet [18]. Due to the reduced local viscosity and thereby less viscous dissipation, the flow on the non-Newtonian side is consequently faster. As a result, the non-Newtonian liquid with higher kinetic energy (KE) wedges unto the Newtonian side from the outer edge of the contact surface, as shown at $T = 1.10$. During the second stage characterized by the formation of axial bulges followed by their shrinking towards the center ($T = 1.10 \sim 2.47$), noticeable geometric asymmetry is generated, with the radial bulge on the non-Newtonian side shrinking more violently,

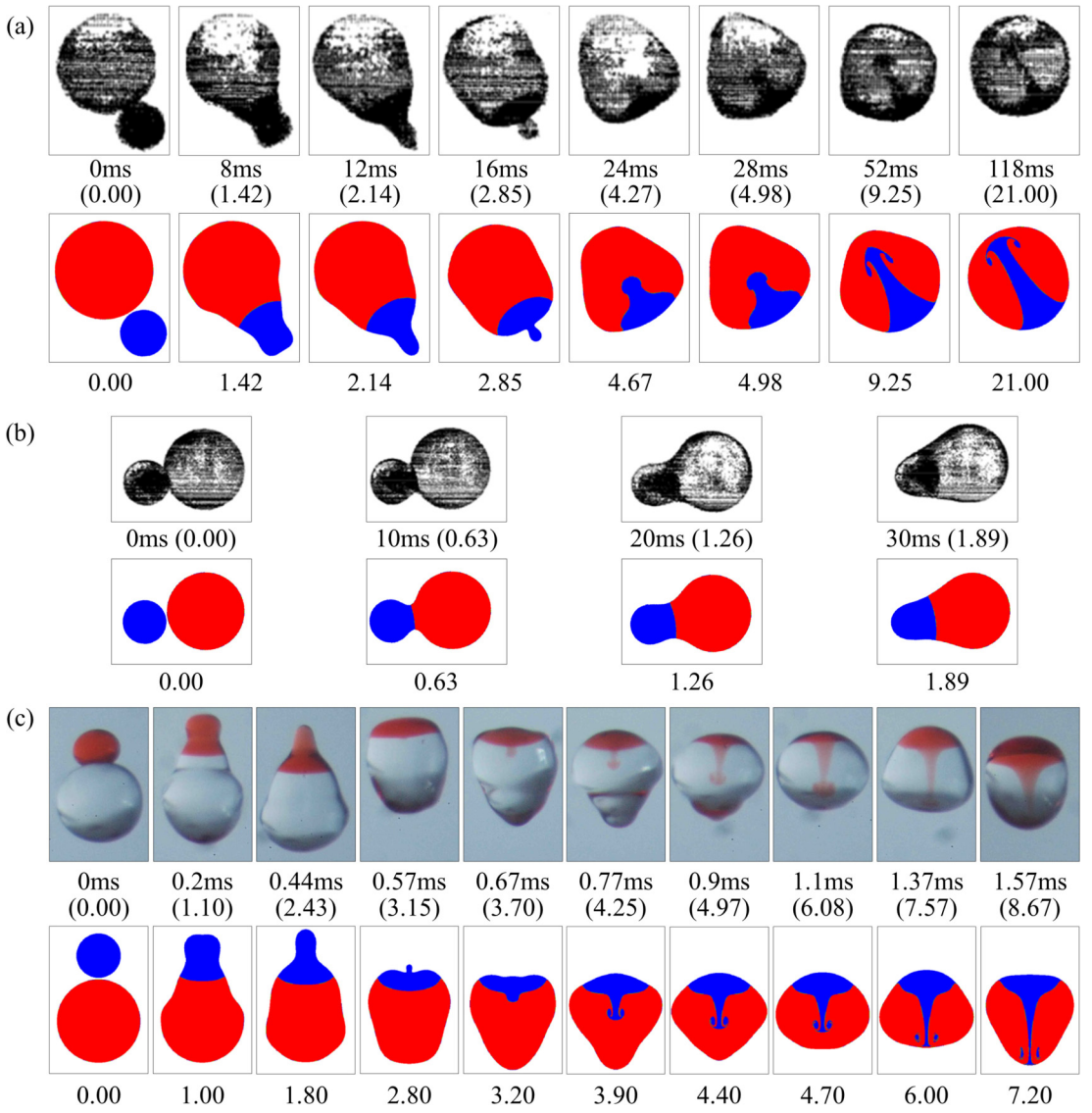

FIG. 2. (Color online) Experimental verification. (a) $\Delta = 2.08$, $\mathrm{Oh} = 0.012$, $\mathrm{We} = 0$, $\rho_d/\rho_a = 1.0$, $\mu_d/\mu_a = 3.3$ (Fig. 2 in Ref. [20]); (b) $\Delta = 1.75$, $\mathrm{Oh} = 0.203$, $\mathrm{We} = 0$, $\rho_d/\rho_a = 0.96$, $\mu_d/\mu_a = 99$ (Fig. 3 in Ref. [20]); (c) $\Delta = 1.86$, $\mathrm{Oh} = 0.006$, $\mathrm{We} = 0.47$ (experiment), $\mathrm{We} = 0$ (simulation), $\rho_d/\rho_a = 833$, $\mu_d/\mu_a = 55.6$ (Type 1 of Fig. 31 in Ref. [19]).

forming a deeper concave at $T = 2.47$. Afterwards, during the long period of oscillation in the third stage ($T > 2.47$), the asymmetry in mixing is further enlarged, eventually resulting in the pattern of internal mixing shown at $T = 13.06$.

For the case with the higher Ohnesorge number of $\mathrm{Oh} = 0.1$, $\mathrm{Oh}_\infty = 0.0015$, as shown in Fig. 3(b), the phenomena are generally the same except that the degree of droplet deformation is smaller due to the higher viscosity, even though

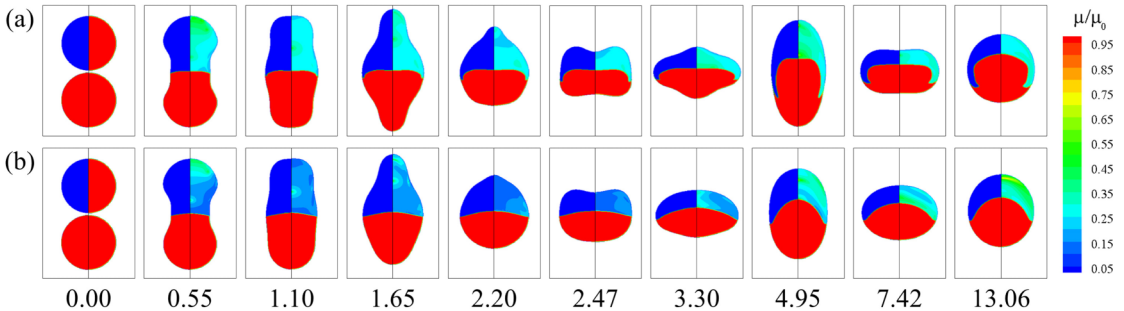

FIG. 3. (Color online) Coalescence between equal-sized non-Newtonian droplet (blue, upper) and Newtonian droplet (red, lower). (a) $\mathrm{Oh} = 0.01$, $\mathrm{Oh}_\infty = 0.0015$; (b) $\mathrm{Oh} = 0.1$, $\mathrm{Oh}_\infty = 0.0015$. In each subfigure, the left half denotes the mixing process, and the right half denotes the normalized viscosity distribution μ/μ_0.

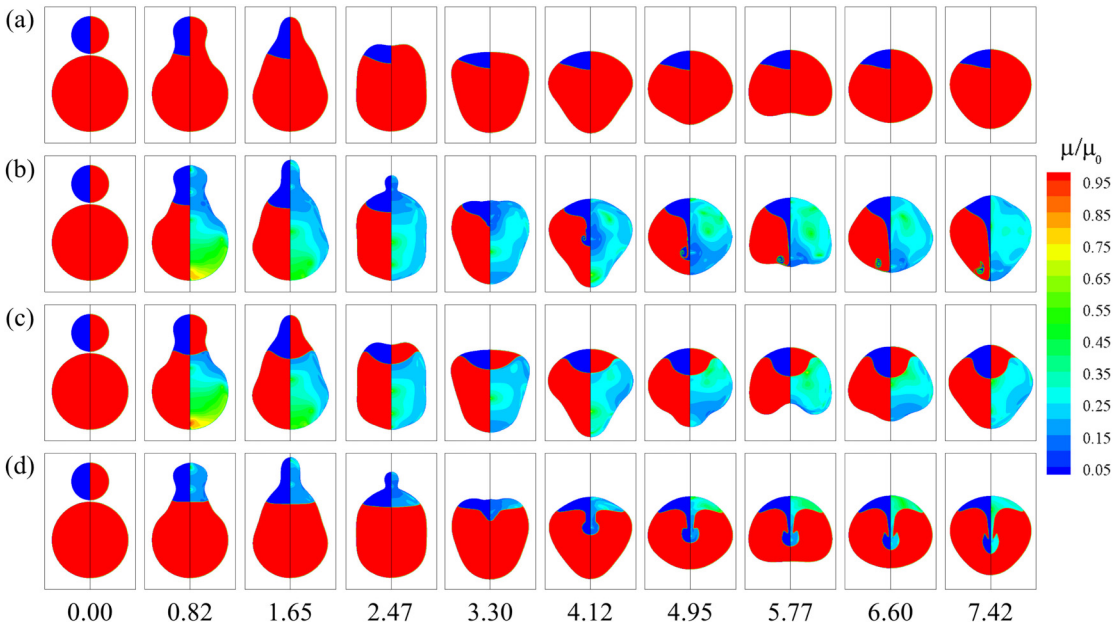

FIG. 4. (Color online) Coalescence between unequal-sized droplets at $\Delta = 2.0$ and $\mathrm{Oh} = 0.05$. (a) Both droplets are Newtonian; (b) both droplets are non-Newtonian ($\mathrm{Oh}_\infty = 0.002$); (c) the larger droplet is non-Newtonian ($\mathrm{Oh}_\infty = 0.002$); (d) the smaller droplet is non-Newtonian ($\mathrm{Oh}_\infty = 0.002$). In each subfigure, the left half denotes the mixing process, and the right half denotes the normalized viscosity distribution μ/μ_0.

the viscosity difference between the droplets is larger. Consequently, while mixing of equal-sized droplets can be enhanced by breaking the symmetry of viscosity via the non-Newtonian, shear-thinning, effect, the strong mixing numerically identified by Blanchette [24] is not likely to occur by further changing the non-Newtonian rheology. This is because in Ref. [24], the Marangoni effect due to difference in surface tension is the driving force to promote mixing and the effect was found to generate rigorous internal motion within the coalesced, while the shear-thinning effect affects the mixing process in a passive way by modifying the local viscosity to modulate the internal flow strength to a minor extent.

C. Coalescence between unequal-sized droplets

Figure 4 shows four prototype cases for the coalescence between two unequal-sized droplets of $\Delta = 2.0$, $\mathrm{Oh} = 0.05$, and $\mathrm{Oh}_\infty = 0.002$. Specifically, Figs. 4(a)–4(d) sequentially show the benchmark case in which both droplets are Newtonian, then both droplets are non-Newtonian, then the smaller droplet is Newtonian and the larger one non-Newtonian, and, finally, the smaller droplet is non-Newtonian and the larger one Newtonian.

It is found that the coalescence between unequal-sized droplets can be also characterized by the three temporal stages identified for the equal-sized cases. Specifically, upon coalescence the surface ruptures and expands radially, leaving a bulge on the side of the smaller droplet during stage 1. Subsequently, the bulge shrinks rapidly into the coalesced mass until it completely disappears during stage 2. The droplet then oscillates and internal mixing further develops during stage 3.

For case (a), it is well known that internal mixing can only form at sufficiently low Ohnesorge numbers [19,20,22,23], and it cannot form at $\mathrm{Oh} = 0.05$. For case (b) where both droplets are non-Newtonian fluid, with large Oh at small shear rates but sufficiently small Oh_∞ at large shear rates, a significant, jetlike mixing forms. This result is expected because internal mixing can be promoted by shear thinning to reduce the local viscosity. However, such a large degree of promotion is somewhat unexpected as the droplets are initially stationary and the internal flow is driven by surface tension alone.

To identify the underlying physics, we designed the simulations for cases (c) and (d) by keeping either the smaller or the larger droplet non-Newtonian. It is then seen that significant mixing occurs only if the smaller droplet is non-Newtonian, as otherwise it would just bulge into the larger non-Newtonian droplet, as shown in Figs. 4(d) and 4(c), respectively.

We next note that in the study of Liu *et al.* [23], the important role of the surface energy associated with the merged interface was identified in forming the jetlike mixing structure subsequent to the coalescence of initially stationary droplets of a Newtonian fluid. Because of the absence of initial kinetic energy, surface energy is the only source in forming the mixing jet, which requires the concentration of the kinetic energy of the internal flow. Increasing the flow viscosity will increase viscous dissipation of the internal flow and thereby suppressing the mixing. Following the same line of thought, we show the evolution of the kinetic energy, normalized by the initial surface energy of the droplets, for the four cases in Fig. 5. It is seen that for the benchmark case (a), the total energy of the two droplets (TKE) increases immediately after surface merging and reaches a maximum at the end of stage 2 ($T = 2.3$). During stages 1 and 2, most of the TKE is from

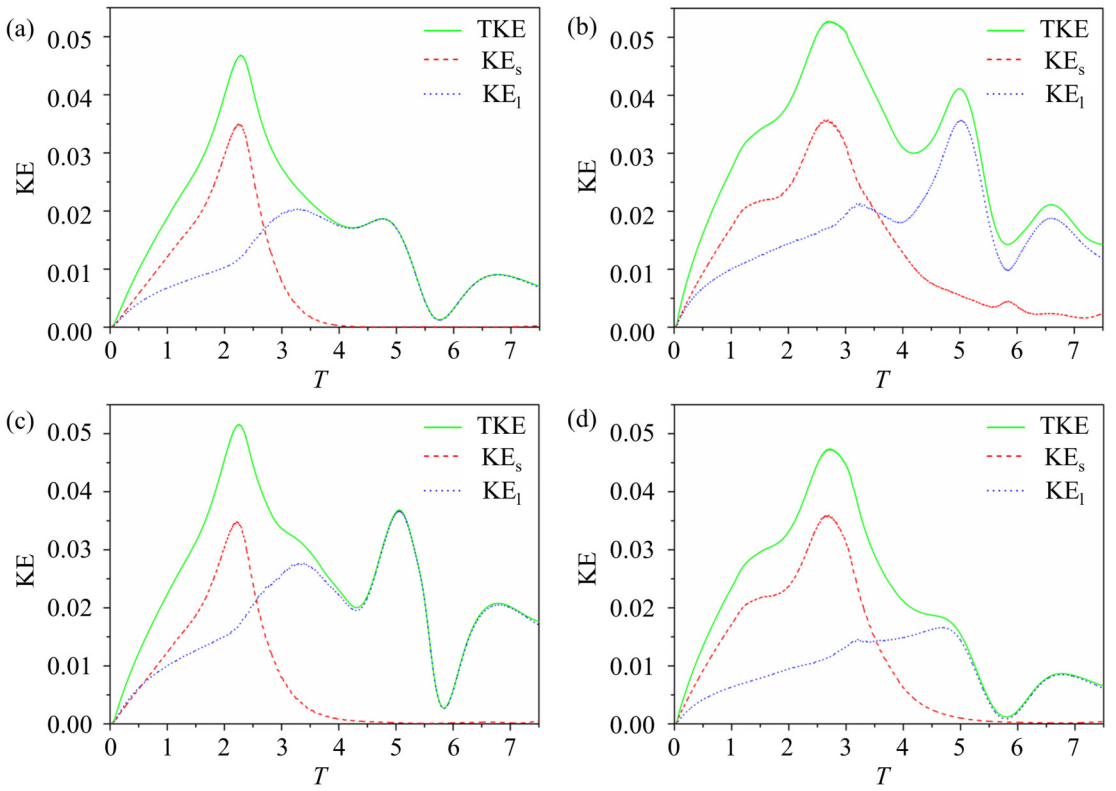

FIG. 5. (Color online) Comparison of evolutions of the total kinetic energy (TKE), the kinetic energy of the smaller droplet (KE$_s$), and the kinetic energy of the larger droplet (KE$_l$) between four cases shown in Fig. 4.

that of the smaller droplet (KE$_s$) instead of the larger droplet (KE$_l$). Subsequently, TKE decreases as the deformed surface tends to recover to the spherical shape in an oscillatory manner in stage 3. The peak value of TKE is less than 0.05, indicating only a small portion of the surface energy is transformed into kinetic energy during the process. For case (c), KE$_l$ sees an obvious increase compared to case (a), while KE$_s$ remains almost unchanged. However, the obvious jetlike mixing is still absent in this case although the viscosity in the larger droplet is significantly lower than that in case (a), implying that the flow motion in the smaller droplet may play a more important role. For cases (b) and (d), it is surprising to observe that although the first peaks of TKE and KE$_s$ are postponed slightly as the smaller droplet takes more time to deform during stages 1–2, there are only slight increases in both TKE and KE$_s$, and the decrease in KE$_l$ is also not significant compared to case (a). Therefore, it is unlikely to correlate the formation of the jetlike mixing with the significant rise in kinetic energy as a result of reduced viscous dissipation by the shear-thinning effect.

By comparing the evolution of the droplet shape, particularly that during the period between $T = 1.65$ and $T = 2.47$, in cases (b) and (d) with those in cases (a) and (c), it is seen that the rapid contraction of the axial bulge under surface tension during stage 2 seems to be crucial in forming the jetlike mixing, as it generates the necessary axial momentum to push the bulge into the larger droplet during stage 3. For case (c), although the viscosity in the larger droplet is greatly reduced by shear thinning, the bulge contraction during stage 2 is not remarkable enough since the high viscosity of the bulge tends to suppress the momentum concentration. However, for case (d), the shear-thinning effect in the smaller droplet causes a significant decrease of the viscosity in the bulge and in the vicinity of the contact surface where the shear rates are higher than that in the interior of the larger droplet. As a result, the axial bulge is able to maintain its larger curvature during stage 2, and the rapid contraction of the bulge into the larger droplet eventually leads to the higher concentration of the axial momentum and, consequently, the jetlike mixing in stage 3. In addition, the higher viscosity of the larger droplet in case (d) than in case (b) suppresses the subsequent development of the jetlike mixing so the penetration depth of the "jet" is substantially larger in case (b) than in case (d).

D. Effect of the extent of shear thinning

To further substantiate the above interpretation on the distinctly different roles of the shear-thinning effect in the smaller and larger droplets, a large number of simulations with various parameters in the shear-thinning constitutive relation Eq. (1) have been conducted. Although the four parameters, μ_∞, λ_{CY}, n, and a, are all related to the extent of the shear-thinning effect, only λ_{CY} and n are chosen to vary in the present study, as λ_{CY} controls the starting shear rate in the power-law region and n determines the rate that the viscosity changes with shear in the region. We neglect the influence of μ_∞ and a because the shear rates appearing in the present problem are not sufficiently high to signify μ_∞ and a plays a similar role as n in affecting the shear-thinning relation at relatively small shear rates. In Fig. 6, the mixing pattern at $T = 8.25$ with different λ ($\lambda = \lambda_{CY}/T_{OSC}$) and n are

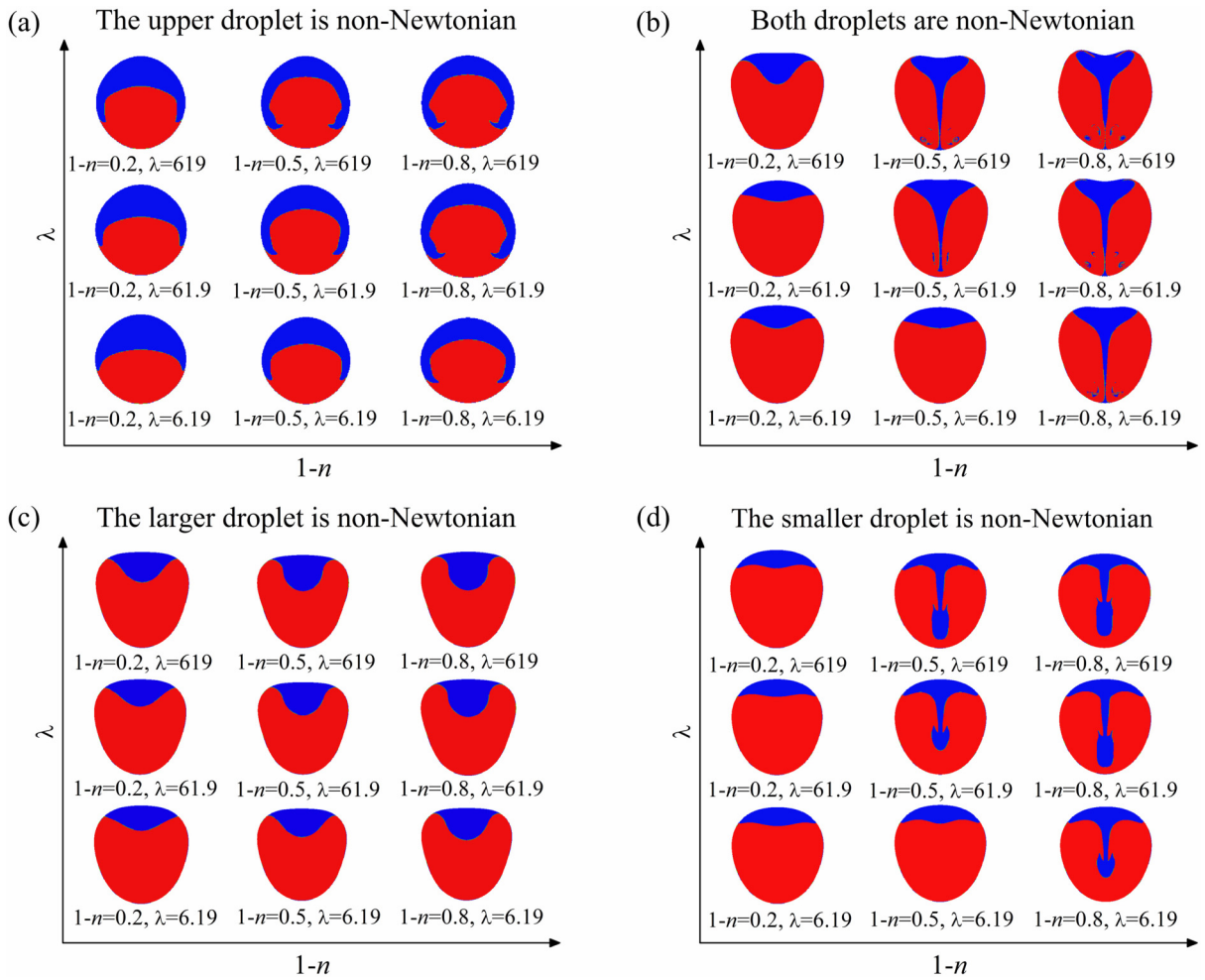

FIG. 6. (Color online) Effect of the extent of shear-thinning on the results. Each figure illustrates the mixing pattern at $T = 8.25$. (a) Equal-sized, the blue (upper) droplet is non-Newtonian; (b) unequal-sized, both droplets are non-Newtonian; (c) unequal-sized, the larger droplet is non-Newtonian; (d) unequal-sized, the smaller droplet is non-Newtonian.

presented and compared with the cases shown in Figs. 3(a), 4(b), 4(c), and 4(d), respectively. It is seen that with increasing either $(1 - n)$ or λ, the shear-thinning effect is increased and the mixing process is accordingly enhanced. Therefore, the phenomena identified in the present simulation should exist for general shear-thinning fluids, in spite of some quantitative differences, as long as the extent of shear-thinning reaches a certain level.

To further study the influence of the extent of shear thinning effect on the evolution of internal mixing, the four cases at the top right corner in Fig. 6(b) are chosen for comparison, in which both droplets are non-Newtonian fluid. In Fig. 7, case (a) serves as the benchmark with $\lambda = 61.9, 1 - n = 0.5$, cases (b) with $\lambda = 619, 1 - n = 0.5$ and (c) with $\lambda = 61.9, 1 - n = 0.8$ have stronger shear-thinning effects than case (a) because of either larger λ or $1 - n$, and case (d) with $\lambda = 619, 1 - n = 0.8$ has the highest shear-thinning effect of the four cases. It is seen that the first two stages of the coalescence process ($T = 0.00 \sim 2.47$) show no obvious difference for all the cases, while during the third stage the internal jet tends to be thicker and develops more rapidly with increasing extent of shear-thinning effect (either in λ or $1 - n$). However, as the shear-thinning effect is sufficiently strong such as in cases (b)–(d), further scrutinizing minor difference between the mixing structures is of little physical importance, since the viscosity around the rushing jet is approaching μ_∞ due to the high local shear rates and large λ and $1 - n$.

E. Schematic regime diagrams

Synthesizing the above results, we show in Fig. 8 the schematic regime diagrams for different combinations of Newtonian and non-Newtonian droplets, with the representative parameters in Eq. (1) chosen as $\lambda = 61.9, n = 0.5, a = 0.557$, and $\mathrm{Oh}_\infty = 0.002$. As shown in Fig. 8(a) where both droplets are Newtonian, three types of mixing are observed as "jet", "bulge", and "dome"-like patterns. It is seen that internal mixing is promoted with increasing Δ and decreasing Oh. However, jetlike mixing occurs only in relatively narrow ranges of Δ and Oh. When both droplets are non-Newtonian, regimes for the jet- and bulgelike mixing are substantially expanded to much higher Ohnesorge numbers. For example, at $\Delta = 2.5$, jetlike mixing can be formed even at $\mathrm{Oh} = 0.1$, which is an order of magnitude higher than the critical Ohnesorge number for Newtonian droplets at the same size ratio, as shown in Fig. 8(a).

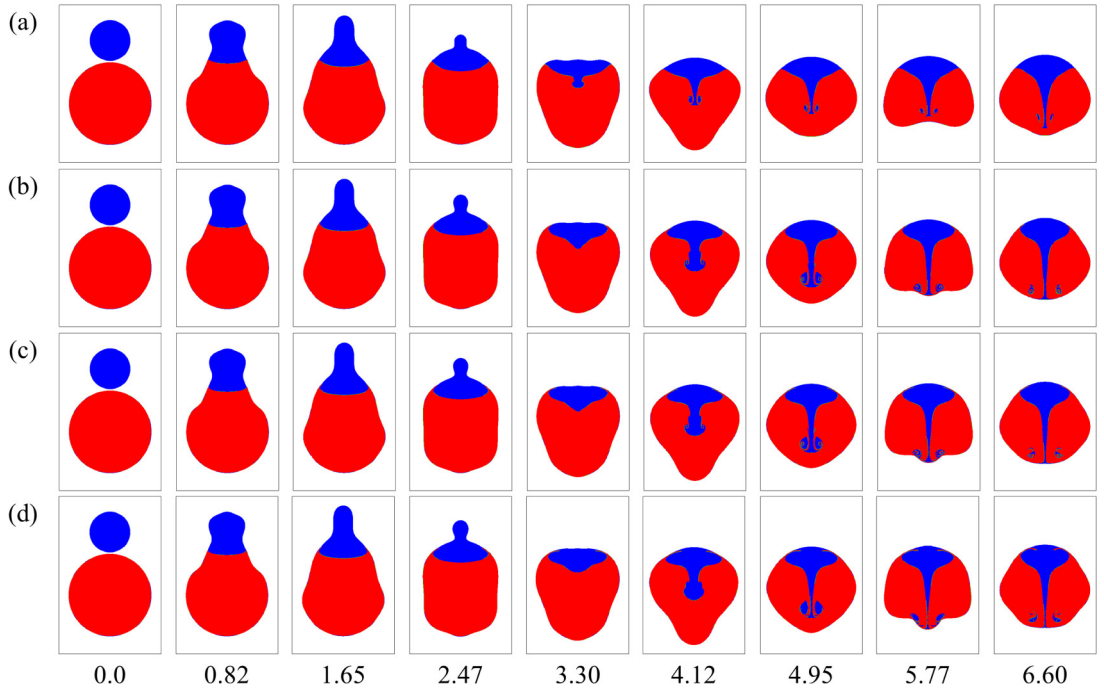

FIG. 7. (Color online) Effect of the extent of shear thinning on the dynamic mixing process: (a) $\lambda = 61.9$, $1 - n = 0.5$; (b) $\lambda = 619$, $1 - n = 0.5$; (c) $\lambda = 61.9$, $1 - n = 0.8$; (d) $\lambda = 619$, $1 - n = 0.8$. In all cases, both droplets are non-Newtonian fluid with $\Delta = 2.0$, $\mathrm{Oh} = 0.05$, and $\mathrm{Oh}_\infty = 0.002$

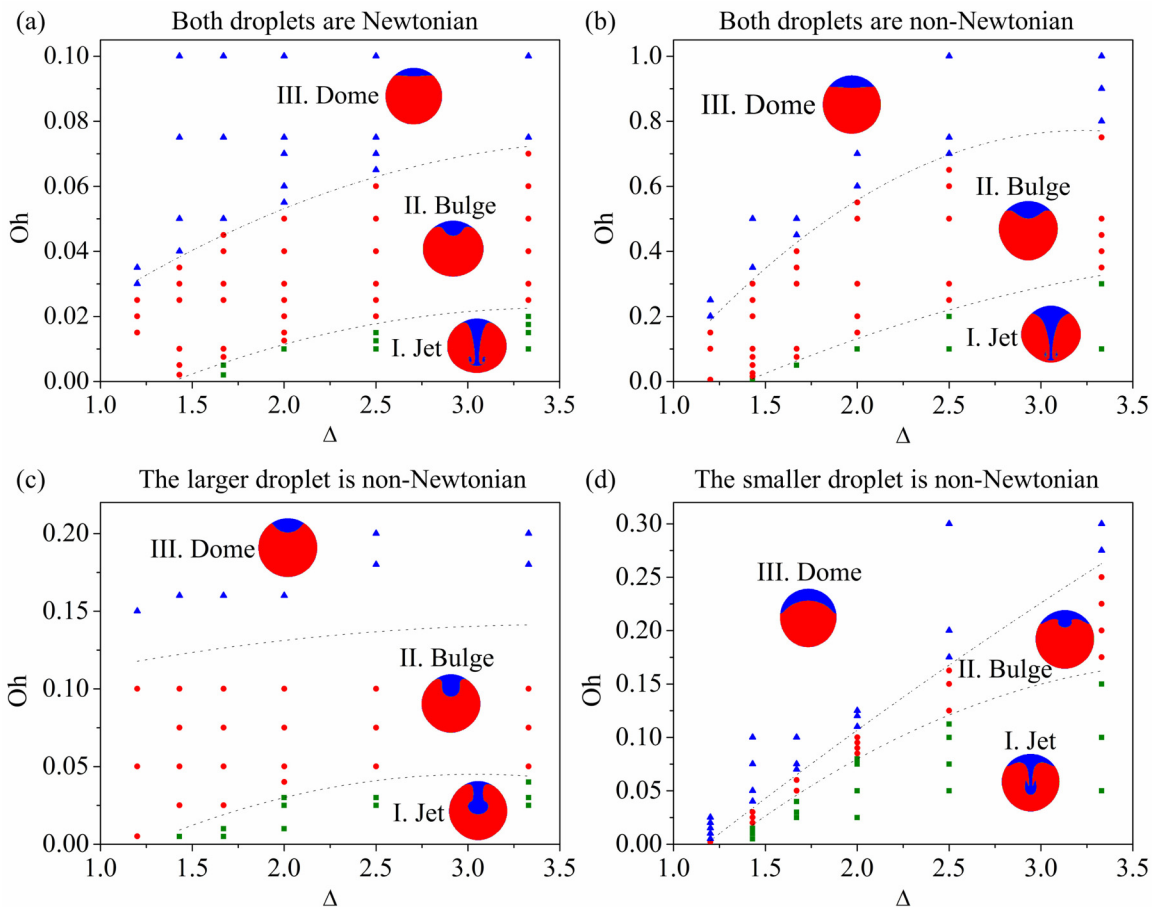

FIG. 8. (Color online) Schematic regime diagrams for different combinations of Newtonian and non-Newtonian droplets. For shear-thinning fluid, parameters in Eq. (1) are chosen as $\lambda = 61.9$, $n = 0.5$, $a = 0.557$, and $\mathrm{Oh}_\infty = 0.002$.

When only one of the droplets is non-Newtonian, Figs. 8(c) and 8(d) show that although the jet- and bulgelike mixing is not so obvious as the "both non-Newtonian" case (b), the enhancement of internal mixing is nevertheless still significant as compared to the "both Newtonian" case (a). Specifically, if the larger droplet is non-Newtonian, the regime for the jet- and bulgelike mixing is enlarged slightly, although the jetlike structure is less prominent as it is chunky with a bulb-shaped head. On the other hand, if the smaller droplet is non-Newtonian, the regime for jetlike mixing is significantly expanded, with the smaller droplet appearing to be nailed onto the larger one. As discussed, the jetlike mixing in cases (b) and (d) originates from the second stage of the coalescence, when the bulge on the side of smaller droplet tends to "penetrate" axially into the larger non-Newtonian droplet. However, compared to case (b), the penetration tends to expand more radially in case (d) as a result of the much higher axial resistance due to the high viscosity in the larger, Newtonian droplet.

IV. CONCLUSIONS

In the present study, the coalescence of two initially stationary droplets is numerically studied by using the LBM. The shear-thinning effect, described by the Carreau-Yasuda model, is implemented in the framework of LBM by modifying the viscosity-related terms into shear-rate-dependent ones. To visualize internal mixing within the coalesced droplet, separate groups of massless tracing particles for each droplet are tracked by using the fourth-order Runge-Kutta method.

The simulation shows that the shear-thinning effect from one of the equal-sized droplets is capable of breaking the symmetry so the non-Newtonian droplet tends to wrap around the Newtonian one as a result of the reduced viscous dissipation and hence the faster shear flow on the non-Newtonian side of the contact surface. However, strong mixing is not likely to occur for equal-sized droplet coalescence because the surface tension is the dominant driving force and viscous dissipation affects passively the mixing process by modulating the internal flow strength to a minor extent.

For unequal-sized droplets, however, the shear-thinning effect from either of the droplets is shown to be capable of promoting mixing as a result of the dramatic reduction in viscosity during coalescence. However, jetlike mixing can be significantly facilitated only if the smaller droplet is non-Newtonian regardless of whether the larger droplet is Newtonian or non-Newtonion. This is because the shear-thinning effect imposed on the smaller droplet reduces the viscous dissipation inside the axial bulge, whose surface-tension driven contraction along the axial direction to the larger droplet is found to play a crucial role in jetlike mixing. A parametric study on the influence of the Carreau-Yasuda model on the present problem shows that the phenomena identified should be universal to a wide range of shear-thinning fluids once the extent of shear-thinning reaches a certain level, and the internal jet tends to be thicker and develops more rapidly with increasing extent of shear-thinning effect, while the difference becomes very minor when the shear-thinning effect is sufficiently strong.

ACKNOWLEDGMENTS

The work was supported in part by the Hong Kong Research Grants Council/General Research Fund (operating under Contract No. PolyU 152217/14E) and in part by a Central Research Grant of the Hong Kong Polytechnic University (operating under Contract No. G-YL42). The collaboration between the Hong Kong Polytechnic University and Tsinghua University was facilitated through the SRFDP & RGC ERG Joint Research Scheme (M-PolyU509/13).

[1] P. R. Brazier-Smith, S. G. Jennings, and J. Latham, Proc. R. Soc. Lond. A **326**, 393 (1972).
[2] G. Brenn and A. Frohn, J. Aerosol. Sci. **20**, 1027 (1989).
[3] N. Ashgriz and J. Y. Poo, J. Fluid Mech. **221**, 183 (1990).
[4] J. Qian and C. K. Law, J. Fluid Mech. **331**, 59 (1997).
[5] K. D. Willis and M. E. Orme, Exp. Fluids **29**, 347 (2000).
[6] K. L. Pan, C. K. Law, and B. Zhou, J. Appl. Phys. **103**, 064901 (2008).
[7] C. L. Tang, P. Zhang, and C. K. Law, Phys. Fluids **24**, 022101 (2012).
[8] F. Mashayek, N. Ashgriz, W. J. Minkowycz, and B. Shotorban, Int. J. Heat Mass Transfer **46**, 77 (2003).
[9] K. N. Premnath and J. Abraham, Phys. Fluids **17**, 122105 (2005).
[10] N. Nikolopoulos, K. S. Nikas, and G. Bergeles, Comput. Fluids **38**, 1191 (2009).
[11] N. Nikolopoulos and G. Bergeles, Int. J. Heat Mass Transfer **54**, 678 (2011).
[12] N. Nikolopoulos, G. Strotos, K. S. Nikas, and G. Bergeles, Int. J. Heat Mass Transfer **55**, 2137 (2012).
[13] K. Sun, M. Jia, and T. Y. Wang, Int. J. Heat Mass Transfer **58**, 260 (2013).
[14] K. Sun, M. Jia, and T. Y. Wang, Int. J. Heat Mass Transfer **70**, 629 (2014).
[15] D. Lycett-Brown, I. Karlin, and K. H. Luo, Commun. Comput. Phys. **9**, 1219 (2011).
[16] D. Lycett-Brown, K. H. Luo, R. H. Liu, and P. M. Lv, Phys. Fluids **26**, 023303 (2014).
[17] X. D. Chen, D. J. Ma, P. Khare, and V. Yang, in *Proceedings of the 49th AIAA Aerospace Sciences Meeting including the New Horizons Forum and Aerospace Exposition, Orlando, 2011* (American Institute of Aeronautics and Astronautics, Reston, 2011).
[18] P. Zhang and C. K. Law, Phys. Fluids **23**, 042102 (2011).
[19] C. K. Law, AIAA J. **50**, 19 (2012).
[20] A. V. Anilkumar, C. P. Lee, and T. G. Tang, Phys. Fluids A **3**, 2587 (1991).
[21] C. L. Tang, Z. H. Huang, P. Zhang, and C. K. Law (unpublished).
[22] M. R. Nobari and G. Tryggvason, NASA Technical Report No. 19950007240 (1994).
[23] D. Liu, P. Zhang, C. K. Law, and Y. C. Guo, Int. J. Heat Mass Transfer **57**, 421 (2013).
[24] F. Blanchette, Phys. Rev. Lett. **105**, 074501 (2010).

[25] M. Motzigemba, N. Roth, D. Bothe, H. J. Warnecke, J. Prüss, K. Wielage, and B. Weigan, in Proceedings of the 18th Annual Conference Liquid Atomization and Spray Systems (ILASS-Europe), Zaragoza, 2002 (unpublished).
[26] C. Focke and D. Bothe, J. Non-Newtonian Fluid Mech. **166**, 799 (2011).
[27] C. Focke and D. Bothe, Phys. Fluids **24**, 073105 (2012).
[28] C. Focke, M. Kuschel, M. Sommerfeld, and D. Bothe, Int. J. Multiphase Flow **56**, 81 (2013).
[29] T. Lee and L. Liu, J. Comput. Phys. **229**, 8045 (2010).
[30] T. Lee, Comput. Math. Appl. **58**, 987 (2009).
[31] E. Aharonov and D. H. Rothman, Geophys. Res. Lett. **20**, 679 (1993).
[32] E. S. Boek, J. Chin, and P. V. Coveney, Int. J. Mod. Phys. B **17**, 99 (2003).
[33] J. Boyd, J. Buick, and S. Green, J. Phys. A: Math. Gen. **39**, 14241 (2006).
[34] S. Khali, R. Nebbali, D. E. Ameziani, and K. Bouhadef, Phys. Rev. E **87**, 053002 (2013).
[35] M. P. Escudier, I. W. Gouldson, A. S. Pereira, F. T. Pinho, and R. J. Pool, J. Non-Newtonian Fluid Mech. **97**, 99 (2001).